Arch. Hydrobiol. 137 1 1–23 Stuttgart, July 1996

Inundation patterns in the Pantanal wetland of South America determined from passive microwave remote sensing

Stephen K. Hamilton[1,3], Suzanne J. Sippel[1,3] and John M. Melack[1,2]

University of California, Santa Barbara

With 10 figures and 1 table in the text

Abstract: Seasonal inundation determines the structure and function of tropical floodplain ecosystems, and therefore information on the spatial and temporal variability of inundation is fundamental to understand and manage these ecosystems. This study uses the 37-GHz polarization difference observed by the Scanning Multichannel Microwave Radiometer (SMMR: Nimbus-7 satellite) to reveal inundation patterns in the Pantanal, a vast savanna floodplain located largely in Brazil. We calculated inundation area separately for 10 subregions using mixing models that account for the major landscape units with distinctive microwave emission characteristics. Maximum inundation occurred as early as February in the northern subregions and as late as June in the south, reflecting the delayed drainage of the region. As much as 131,000 km^2 was inundated annually during the 9 years of SMMR observations (1979–87). Monthly estimates of the total area inundated in the region varied from 11,000–110,000 km^2, averaging 53,000 km^2. We reconstructed regional inundation patterns over the past 95 years from the correlation between the Paraguay River stage and total inundation area during the SMMR period. Both the maximum and minimum inundation area showed large interannual variability.

Introduction

Information on inundation patterns is required for understanding the hydrology, biogeochemistry and ecology of the extensive floodplains of tropical re-

[1] **Authors' addresses:** Marine Science Institute and

[2] Department of Biological Sciences, University of California, Santa Barbara, California 93106-9610 USA.

[3] Present address: W. K. Kellogg Biological Station, Michigan State University, Hickory Corners, MI 49060-9516 USA.

0003-9136/96/0137-0001 $ 5.75

gions (RICHEY et al. 1991, BARTLETT & HARRISS 1993, JUNK 1993). Such information is also essential to assess the viability and environmental impacts of proposed development projects that entail the regulation of floodplain rivers (e.g., SUTCLIFFE & PARKS 1987, BUCHER et al. 1993). River stage records have historically provided the best available information on inundation patterns in floodplains, but for many tropical regions stage records are often incomplete and limited in spatial coverage, and may not represent flooding conditions in areas distant from the main river channels. Remote sensing now offers the opportunity for synoptic observation of inundation patterns. However, the application of optical remote sensing systems to observe inundation dynamics in wetlands has been hampered by persistent cloud cover and dense vegetation canopies overlying the water (MELACK et al. 1994). In contrast to optical systems, passive microwave remote sensing from satellites can detect inundation when clouds and vegetation are present and can thus provide a multi-year record of inundation area in large wetlands (GIDDINGS & CHOUDHURY 1989, CHOUDHURY 1991, SIPPEL et al. 1994).

In this study, we present data on seasonal and interannual variation in inundation area in the Pantanal, one of the world's largest tropical wetlands. These data are derived from passive microwave emission measured at 37 GHz by a satellite-borne sensor, the Scanning Multichannel Microwave Radiometer (SMMR). Our methods are based on the approach described by SIPPEL et al. (1994), who determined fractional inundation area for a reach of the central Amazon floodplain by using mixing models to account for the major landscape units with distinctive microwave emission characteristics. The passive microwave observations provide an unprecedented view of inundation dynamics in large, remote wetlands such as the Pantanal.

Study area

The Pantanal is a vast savanna wetland in tropical South America, occupying an area of 137,000 km^2 (approximately 450 by 300 km) in the upper Paraguay River basin (Fig. 1). Most of the region is in Brazil, with smaller areas to the west in Bolivia and Paraguay. A mosaic of alluvial fans of Pleistocene origin fills the Pantanal depression (KLAMMER 1982), where elevation ranges from 85–150 m and the land slopes gently toward the Paraguay River. The upland drainage basin surrounding the Pantanal occupies 359,000 km^2 and consists of elevated plateaus and low mountains to the north and east (250–1200 m elevation) and flat plains to the west. Human population density is very low within the Pantanal (<2/km^2: BRAZIL 1982), where the main economic activity is cattle ranching.

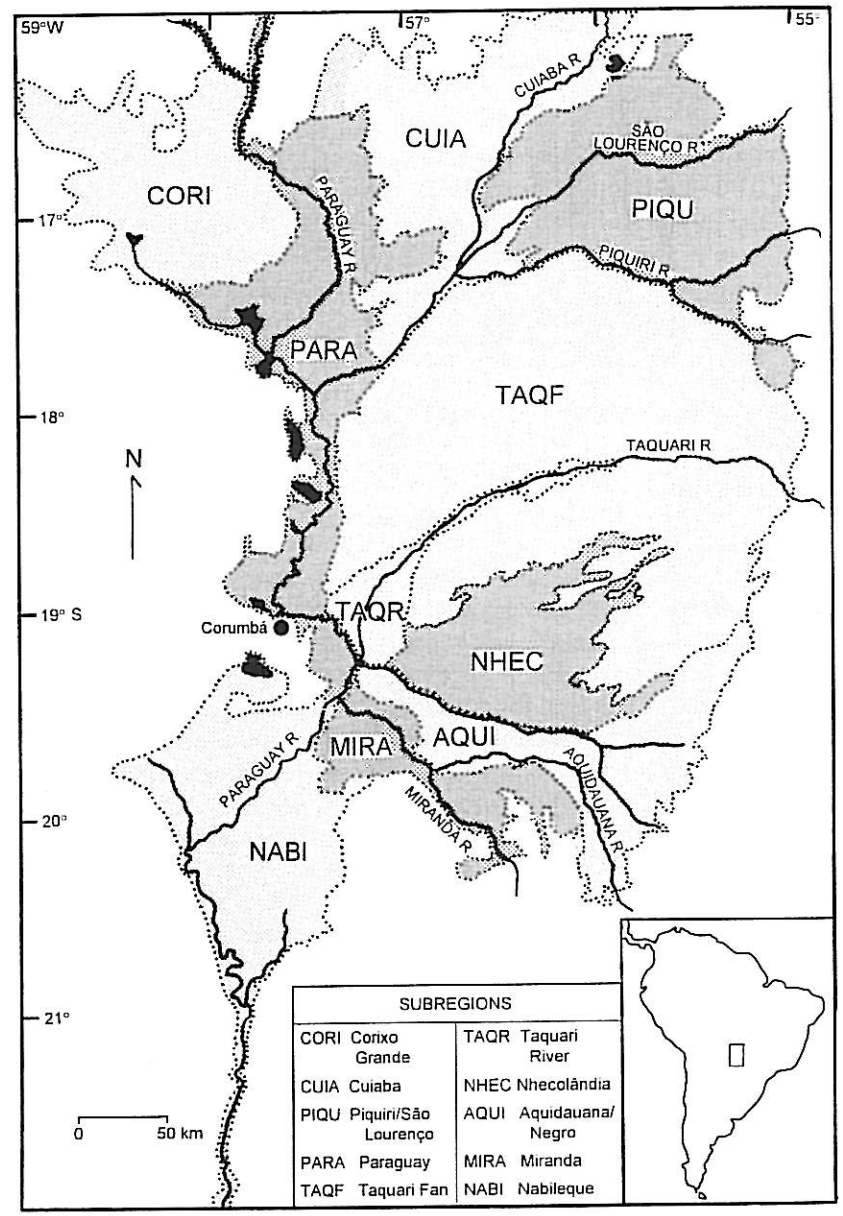

Fig. 1. Major rivers and subregions of the Pantanal wetland.

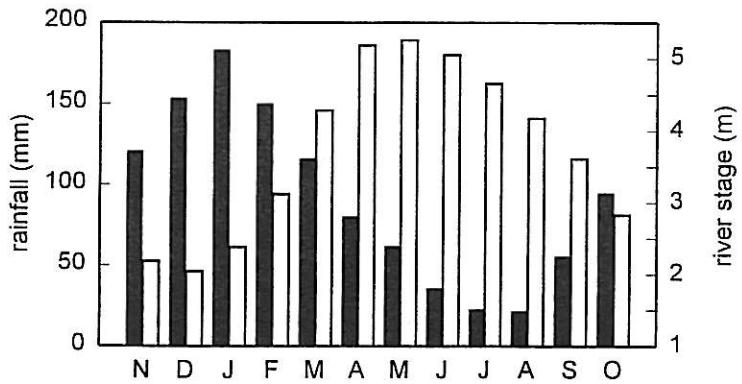

Fig. 2. Mean monthly rainfall at Corumbá (filled bars) and mean monthly stage (water level; open bars) of the Paraguay River at Ladário (near Corumbá). Rain data are for 1912–71 (UNESCO 1973) and stage data are for 1979–87 (data provided by the Brazilian Navy at Ladário).

The climate of the Pantanal is tropical with a marked wet season (BRAZIL 1979). Annual rainfall is generally 1000–1700 mm across the region, with most rain falling between November and March (Fig. 2). Rainfall is highest in some parts of the surrounding uplands, particularly in the north, and lowest in the floodplain areas of the southwest Pantanal. The hydrology of the main river systems remains unregulated. Flooding in the region is distinctly seasonal, although the flooding period tends to be delayed after the rains due to slow passage of floodwaters through the Pantanal (BRAZIL 1979). Many areas are flooded by riverine overflow and are thus true floodplains, while other areas normally flood with local rainfall, although their geomorphological origin may be alluvial (HAMILTON et al., in press). The water in most floodplain areas tends to flow slowly in a characteristic direction, at least during high water. Water depth is usually <6 m outside of the river channels and is most commonly <2.5 m on the floodplains (HAMILTON et al. 1995).

The Paraguay River runs from north to south along the western side of the Pantanal, collecting water from the various tributaries and non-channelized floodplain flow paths (Fig. 1). The slope of the Paraguay River in the Pantanal is 2.5 cm/km (BRAZIL 1979). Seasonal variation in the discharge of the Paraguay River is strongly damped by the storage of water on adjacent floodplains, and in the southern Pantanal the flood wave is delayed by up to 4–5 months after the peak rainfall (Fig. 2). The mean annual discharge of the Paraguay River is 1260 m^3/s at Corumbá, where the river carries 80 % of the total outflow from the region, and interannual variation in discharge is large (BRAZIL 1979). Water levels of the tributaries are controlled by the Paraguay River near their confluences because of the gentle elevational gradients. The peak discharge of these tributaries tends to occur earlier than that of the Paraguay River, and the later rise of the Paraguay impounds the lower courses of the tributaries, decreasing their current and sometimes even reversing their flow temporarily (HAMILTON et al., in press).

Savanna and mixtures of grassland with semideciduous forest are the most common vegetation types, although gallery forest occurs along rivers (PRANCE & SCHALLER 1982, RATTER et al. 1988, PRADO et al. 1992, JUNK 1993). Trees and shrubs are often present but usually have sparse canopies in areas subject to inundation, allowing herbaceous plants to coexist in the understory. Extensive stands of trees dominated by a single species are common. The most important of these species include the Cambará (*Vochysia* spp.), which often grows in dense patches throughout the region, and the Carandá palm (*Copernicia australis*) and Paratudo (*Tabebuia caraiba*), which commonly occur as more open stands in the southern Pantanal. Human impact on vegetation in the Pantanal has occurred mainly through the introduction of cattle and the use of fire during the last 200 years, which have influenced the nature and distribution of vegetation (PRANCE & SCHALLER 1982, WILCOX 1992).

Aquatic or semi-aquatic vascular plants occur almost everywhere surface water persists for more than a few weeks, and floating and rooted emergent forms often cover much of the water surface (PRANCE & SCHALLER 1982, POTT et al. 1989). Floating emergent plants such as *Eichhornea azurea, E. crassipes, Scirpus cubensis,* and *Salvinia* spp. tend to dominate in more deeply flooded environments. Rooted emergent species with more vertical, erect stems colonize areas of shallower water, and sometimes develop extensive stands of one or a few species, including *Cyperus giganteus, Thalia geniculata, Typha domingensis, Pontederia cordata* var. *lanciofolia, Ipomoea* sp., *Polygonum* spp., *Oryza* sp., and *Paspalum* spp.

Passive microwave sensor systems and data

Passive microwave sensors measure the very faint natural emission of microwave energy from the Earth's surface and atmosphere. Their coarse spatial resolution compared to optical remote sensing systems results because the sensors must integrate the emission over a large area to yield a measurable signal (LILLESAND & KIEFER 1994). Measurements are expressed as brightness temperatures (in Kelvins), and are obtained at several frequencies and at both vertical and horizontal polarizations. The difference between vertically and horizontally polarized brightness temperatures observed by satellite at the 37 GHz frequency (hereafter referred to as ΔT_{obs}) provides a sensitive indicator of the presence of surface water, particularly where water occurs against a background of vegetated land surfaces (GIDDINGS & CHOUDHURY 1989, CHOUD-

HURY 1991). The spatial resolution of the SMMR sensor is approximately 27 km at 37 GHz (FU et al. 1988), and the processed global data sets are gridded into cells of 0.25° latitude by longitude. The theoretical basis for interpretation of 37 GHz emission has been reviewed by CHOUDHURY (1989).

A continuous record of vertically and horizontally polarized 37 GHz observations from satellites is available for late 1978 to the present, at intervals of weekly or better. From December 1978 to August 1987, these data were collected by the SMMR instrument operated on board the Nimbus-7 satellite (GLOERSEN et al. 1984, FU et al. 1988). Similar observations are available from the Special Sensor Microwave/Imager (SSM/I) instruments, which began operation in July 1987 and continue operation now as part of the Defense Meteorological Satellite Program (HOLLINGER et al. 1990).

In this study, we use the SMMR observations for 1979–87, which are drawn from the global data set of the 37 GHz ΔT_{obs} that was originally studied by CHOUDHURY (1989 and 1991). Global SMMR observations are available for approximately 6-day intervals, and are compiled separately for day and night (local equator crossings at noon and midnight). After calculation of ΔT_{obs} for each grid cell from the daytime brightness temperatures, the observations were ranked within each month and the second lowest value (usually out of 4) was selected, thereby yielding one ΔT_{obs} value per month. The screening served to eliminate outlying values that might have resulted from atmospheric scattering by heavy rainfall, or from temporary pooling of water on the land surface after heavy rainfalls.

Methods

Fractional inundation area was calculated for each 0.25° × 0.25° grid cell from the monthly 37 GHz ΔT_{obs}. The algorithms for calculation of fractional inundation area are linear mixing models that incorporate the ΔT values of the major landscape units within a grid cell (SIPPEL et al. 1994):

$$\Delta T_{obs} = f_w(\Delta T_w) + f_{nf}(\Delta T_{nf}) + f_f(\Delta T_f) \quad (1)$$

$$1 = f_w + f_{nf} + f_f \quad (2)$$

where ΔT_{obs} is the ΔT observed by the radiometer, f_w, f_{nf} and f_f are the fractional areas of open water (rivers and lakes), non-flooded land, and seasonally flooded land, respectively, and ΔT_w, ΔT_{nf} and ΔT_f are the ΔT values for open water, non-flooded land, and seasonally flooded land.

We used a ΔT_w value of 60 K, which is the approximate value expected for a smooth water surface (CHOUDHURY 1989). SMMR and aircraft measurements of the ΔT over calm seas support this assumption (HOLLINGER et al. 1990, GLOERSEN et al. 1992). Non-flooded, vegetated land surfaces typically range in ΔT from 4–7 K (JUSTICE et al. 1989). We used a ΔT_{nf} value of 4.2 K, which was determined by averaging

all dates for 16 grid cells of uplands just west of the Pantanal which are not subject to extensive seasonal flooding (s.d. 1.0; N = 1664 observations). The ΔT_{obs} falls to about 4 K over many floodplain areas within the Pantanal that dry completely at low water, indicating that non-flooded floodplain resembles nearby savanna uplands in its radiometric characteristics. In contrast to ΔT_w and ΔT_{nf}, the ΔT_f value is expected to vary among wetland types because of the variable density and structure of emergent vegetation that covers seasonally flooded land. We therefore determined the ΔT_f value empirically for different subregions of the Pantanal, as described below.

The ΔT values of open water, non-flooded land, and flooded land are used together with a measurement of f_w from maps or Landsat Thematic Mapper images to calculate f_f, the fractional inundation area. Simultaneous solution of equations (1) and (2) yields the following equation for f_f:

$$f_f = \frac{\Delta T_{obs} - f_w(\Delta T_w) - \Delta T_{nf} + f_w(\Delta T_{nf})}{\Delta T_f - \Delta T_{nf}} \quad (3)$$

Inundation area includes the open-water area of lakes and river channels, and is thus calculated as the sum of f_w and f_f, times the total grid cell area.

For the purposes of data analysis and presentation, we divided the Pantanal into 10 subregions based on predominant differences in hydrology and geomorphology (Fig. 1). The principal sources used to delineate subregion boundaries were the 1 : 1,000,000 geomorphology and vegetation maps produced by the RADAMBRASIL project from Side-Looking Airborne Radar imagery and ground studies (BRAZIL 1982). We also consulted Landsat TM images from several dates, topographic maps, and ADÁMOLI (1982). In most cases the subregions reflect areas influenced by flooding from a particular river system.

Test cells were identified within each subregion for the determination of ΔT_f. Test cells are representative of the subregion, are almost entirely subject to inundation, and are surrounded by similar landscapes. We found a total of 53 test cells that met these criteria, representing 28 % of the total area of the Pantanal. They were carefully selected based on maps, Landsat TM imagery, and our field experience in the region. We measured the area of open water (lakes and rivers) within each test cell using topographic maps of either 1 : 250,000 (Brazil) or 1 : 50,000 scale (Bolivia and Paraguay). A few cells contained significant upland area that is not subject to inundation, which we also measured from maps. Assuming that the remaining area within the test cell flooded completely during the highest flood years, we used the above equations and the mean of the maximum ΔT_{obs} of the four highest flood years to estimate the ΔT_f of the test cells. For a test cell in the Nhecolândia subregion, which is composed of thousands of small lakes and narrow strips of non-inundable forest (locally called cordilheiras), the forested upland areas were measured from a 1 : 100,000 topographic map and open water was measured from a low-water Landsat TM image (22 Sep 1991).

The ΔT_f values of the test cells were then averaged for each subregion and used in calculations for the remaining cells in the subregion. Two of the subregions (Taquari Fan and Aquidauana/Negro) showed east-west gradients in ΔT_f and therefore instead of using the overall mean ΔT_f, only the ΔT_f values of the closest test cells were averaged to determine the appropriate ΔT_f for a cell. For cells that spanned more than one subre-

gion, a weighted mean ΔT_f was calculated, based on the mean ΔT_f values and fractional areas of each subregion within the cell.

Open water areas for the remaining cells were measured from maps, as for the test cells. Field observations and Landsat TM imagery confirmed that the maps depicted the approximate low-water boundaries of lakes and rivers; seasonally flooded land bordering permanent water bodies tends to be occupied by emergent vegetation, so open-water/floodplain boundaries tend not to change greatly as the water level rises and falls. The particularly small lakes of the Nhecolândia subregion are not accurately depicted on the maps, but are readily visible on Landsat TM images. However, they are too numerous to measure individually across the entire subregion. Therefore, we measured lake area only for the test cell (which contained 964 lakes). Lake area for the remaining cells of Nhecolândia was then determined from the mean low-water ΔT_{obs}, after finding that the mixing models predicted low-water lake area for the test cell if f_f is assumed to be negligible during the dryest periods (measured test-cell f_w = 0.099, predicted f_w = 0.092).

Results and discussion

Effects of atmospheric variability and rainfall

We have found that the seasonal variation in the 37 GHz ΔT_{obs} over the large wetlands of lowland South America is driven by changes in the area inundated rather than by atmospheric variability and local rainfall. Fig. 3 illustrates the effect of inundation on ΔT by comparing the ΔT_{obs} over the floodplain of the Paraguay River north of Corumbá with that over nearby upland grid cells. The mean seasonal patterns of rainfall and river stage in this area are plotted in Fig. 2, showing that the peak in riverine flooding occurs about 4 months later than peak rainfall. The floodplain at this site is flooded by the river rather than by local rainfall, as indicated by the correspondence between river stage and the ΔT_{obs}. The adjacent upland, which is not subject to seasonal inundation, shows relatively little seasonal variation in ΔT_{obs} (Fig. 3). If atmospheric variability or rainfall events produced the seasonal cycle of ΔT_{obs} for the Paraguay River floodplain, then the nearby upland area would show more variability, and the close relationship of the floodplain ΔT_{obs} with river level would not be observed. Similar comparisons yield the same conclusions for the central Amazon floodplain near Manaus (SIPPEL et al. 1994).

The concern has recently been raised that seasonal atmospheric variability can significantly modulate the observed seasonal changes in the 37 GHz ΔT_{obs}, and that correction for this variability might be necessary for studies of seasonal variation in emission from the land surface (KERR & NJOKU 1993). The importance of atmospheric variability in seasonal tropical climates has been postulated based on modeling the effects of seasonal changes in temperature, atmospheric water vapor, and cloud optical thickness on radiative transfer

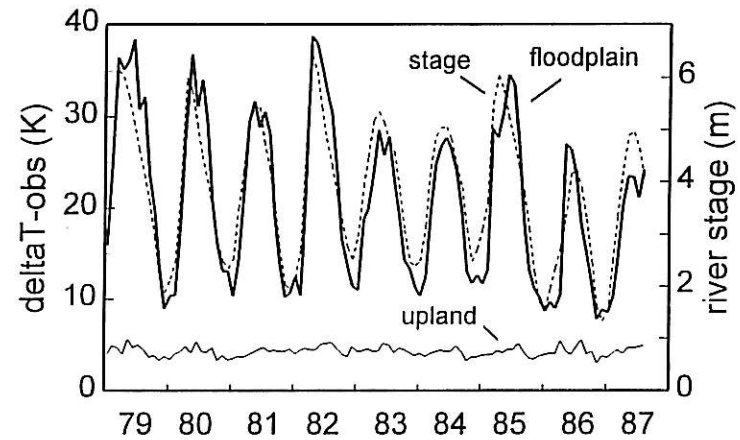

Fig. 3. Comparison of the SMMR 37 GHz ΔT_{obs} (solid lines) over a floodplain and nearby upland area, together with stage (dashed line) of the principal river at the floodplain site, showing that the seasonal cycles in ΔT_{obs} are driven largely by inundation. The floodplain ΔT_{obs} data are means for 4 grid cells located over the Paraguay River floodplain north of Corumbá. Upland ΔT_{obs} data are means for 16 grid cells over the savannas west of the floodplain site. Stage data are monthly means of daily readings for the Paraguay River at Ladário, near Corumbá (data provided by the Brazilian Navy at Ladário).

through the atmosphere, using the Sahel region of Africa as an example (CHOUDHURY et al. 1992, KERR & NJOKU 1993). For studies of South American wetlands, correction of the ΔT_{obs} for the effects of atmospheric variability would not be worthwhile because it would require meteorological data that can only be crudely estimated, and it would introduce new uncertainties into the data set. The above comparison between the ΔT_{obs} over floodplain and upland areas strongly suggests that any effects of seasonal atmospheric variability are not large enough to obscure the effects of seasonal changes in inundation area. Our empirical determination of ΔT_f for each subregion during maximum flooding would help to account for the typical atmospheric conditions during the flood season.

Heavy rainfall events can have contrasting effects on the 37 GHz ΔT_{obs}: liquid hydrometeors in precipitating clouds have a depolarizing effect, reducing the ΔT_{obs} while temporary saturation of soils and pooling of water after a heavy rain could increase ΔT_{obs} (HEYMSFIELD & FULTON 1992). The cloud effects during heavy rains may have been minimized in the monthly data set that we used because of the screening procedure, which would eliminate outliers in a particular month. The lack of strong episodic changes in ΔT_{obs} over upland areas suggests that heavy rainfall events have little effect on the monthly data

set. Saturation of soils by rainfall would persist for longer periods, but HEYMSFIELD & FULTON (1992) have shown that the degree of soil saturation has little effect on ΔT_{obs} over vegetated (grassland) areas. The available evidence suggests that for inundation to significantly increase the ΔT_{obs} over vegetated areas, enough water must accumulate above the soil surface to begin to submerge the vegetation that otherwise effectively attenuates the emission from underlying soil.

Algorithm parameters and sensitivity

As noted above, calculation of inundation area from equation (3) requires knowledge of ΔT_f, the ΔT of inundated areas with emergent vegetation, which we determined empirically for each of the 10 subregions. The results for a total of 53 test cells are summarized in Table 1. Considerable variation in ΔT_f was found among subregions, possibly reflecting variation in the degree of coverage of the water surface with vegetation canopies. However, it is difficult to relate these ΔT_f values to differences in the vegetation or inundation depth among subregions because of the lack of quantitative information on these characteristics at the landscape scale.

East to west gradients of increasing ΔT_f were observed in the test cells of the Taquari fan and Aquidauana/Negro subregions, where inundation depth tends to be greatest toward the west. The highest mean ΔT_f value (51 K) was observed in the Nabileque subregion, where Landsat images indicate that during inundation emergent vegetation is sparser than elsewhere. Several grid

Table 1. Total area, fractional area of open water (lakes and rivers), and the ΔT values of the inundated floodplain (ΔT_f) for each of the 10 subregions in Fig. 1. The ΔT_f values were determined from selected grid cells within each subregion.

Subregion	Total area* (km^2)	Fraction as open water (f_w)	ΔT_f (K)		
			Mean	Range	N
Corixo Grande	11,479	0.021	41.5	37–47	3
Cuiabá	14,406	0.015	20.0	19–21	3
São Lourenço/Piquiri	15,996	0.006	17.3	15–20	4
Paraguay River	16,258	0.089	32.9	25–39	8
Taquari Fan	39,344	0.006	gradient	18–32	20
Taquari River	2,927	0.007	42.9	39–47	2
Nhecolândia	8,623	0.062	33.9	–	1
Miranda	5,035	0.007	18.9		1
Aquidauana/Negro	9,197	0.008	gradient	16–24	3
Nabileque	13,662	0.015	51.0	45–58	8

* The total area is the area of the subregion in Fig. 1, and may not all be subject to inundation.

cells in Nabileque approached a ΔT_{obs} of 60 K at peak inundation, suggesting that they were comprised of a nearly open water surface; these same cells evidently dry almost entirely at low water because their ΔT_{obs} values fall to about 4 K.

A ΔT_f value of 17 K was observed by SIPPEL et al. (1994) for the floodplain of the central Amazon, where inundation depths are generally much greater than in the Pantanal (up to 12 m), but about two-thirds of the floodplain is covered by tall, dense forest. We observed ΔT_f values of 15–20 K in several subregions, generally where inundation depth is shallow (often <1 m) and much of the terrestrial savanna vegetation remains emergent during inundation. Thus it appears that shallow flooding in a sparsely wooded grassland can yield a ΔT_f similar to that produced by much deeper flooding in a largely forested environment.

Error in the calculated inundation area can arise from the five different input terms in equation (3). Propagation of the component errors to estimate the error in f_f is not possible because the variances are indeterminate for some of the components. However, we can perform a sensitivity analysis individually for each component to demonstrate the effects of possible biases in our estimates of the ΔT values for open water, non-flooded land, and seasonally flooded land, and in our measurement of open-water area (f_w).

For the overall region, the sensitivity analysis shows that the calculated inundation area varied by an average of only 1 % when ΔT_w was varied by ± 5 K, and by an average of only 4 % when f_w was varied by ± 30 %. This insensitivity is explained by the low fractional area of open water in the region (overall f_w = 0.02: Table 1). In contrast, varying the ΔT_{nf} by ± 1 K and the ΔT_f by ± 15 % produced greater changes in the calculated inundation area, with the largest absolute effects at low and high ΔT_{obs}, respectively. The magnitude of these effects is shown for a typical annual cycle of ΔT_{obs} in Fig. 4. The effect of error in ΔT_{obs} was evaluated by taking the standard deviation of the 1664 observations over upland areas (1.0 K; see 5.1 above) as an estimate of the overall precision (Fig. 4). This may overestimate random instrument error because it incorporates any temporal variability in emission from the upland areas, although similar variability has been observed over stable regions of the Antarctic ice sheet (GLOERSEN et al. 1992). The sensitivity analyses indicate that the calculation of inundation area in the Pantanal is most sensitive to possible error in the satellite observations and to possible bias in our empirical estimates of ΔT_{nf} and ΔT_f. In other wetlands with a greater proportion of open water, f_w and ΔT_w would become more important.

The geolocation error of the SMMR data analyzed in this study is likely to be about 12 km (CHOUDHURY et al. 1992). Grid cells should therefore be aggregated for data analysis whenever possible to reduce the relative uncertainty in location, and the possible effects of nearby surface features must be consid-

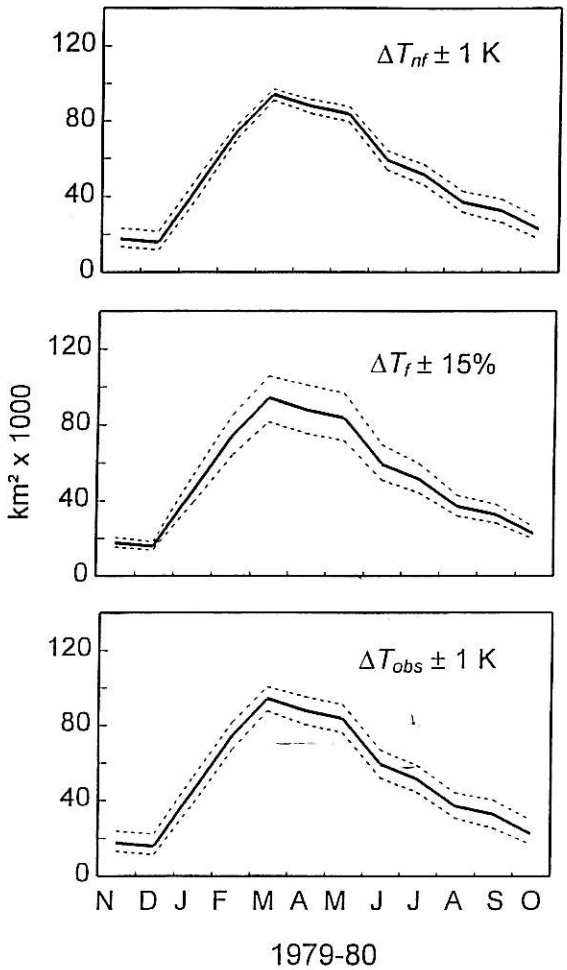

Fig. 4. Sensitivity analysis of the algorithm (equation (3)) for estimation of inundation area from the ΔT_{obs}. A typical annual cycle of the mean ΔT_{obs} for the overall region was selected to illustrate the results. The solid line shows the original inundation area estimates and the dashed lines show the results when an input term was varied. For the present study, these three terms (ΔT_{nf}, ΔT_f and ΔT_{obs}) are potentially most important in the overall error of the algorithm.

ered when the data are interpreted. In this study, the wetland subregions are large and homogeneous enough that geolocation error does not present a problem. Our test cells were located to avoid nearby features that are expected to

show different radiometric characteristics, such as uplands, open water, or neighboring subregions.

The algorithms that we have used in this study could also be applied to the 37 GHz ΔT_{obs} recorded since 1987 by the SSM/I sensors, but the empirically determined SMMR ΔT values are not directly applicable. There are several changes in the design of the SSM/I instrument and in data processing that affect the absolute values of ΔT_{obs} (SPENCER et al. 1989, HOLLINGER et al. 1990, CHOUDHURY et al. 1992, CHOUDHURY 1993). The comparability of SMMR and SSM/I data sets remains under study.

Subregional inundation patterns

Time series for the entire period of the SMMR observations illustrate differences among subregions in the seasonal and interannual variability of inundation area (Fig. 5). The upper limit of the ordinate in each panel is the approximate total area of the subregion. The heights of the peaks show that simultaneous inundation of entire subregions generally does not occur, and that all of the subregions reach a fractional inundation area of at least 50 % for several months in most years. The seasonal cycle of inundation is generally more regular in the northern subregions, which have unimodal flooding patterns with gradual changes. The Miranda and Aquidauana/Negro subregions show more short-term variability, and in some years these subregions lack a distinct seasonal peak of inundation. The Nabileque subregion generally shows gradual changes in inundation area, but is highly variable in the extent of flooding among years.

Differences among subregions are also apparent in the fraction of the total area that remains inundated during the dryest parts of the year. Permanent open-water area is included in the total inundation area, and is thus a baseline area to which the seasonally variable area of inundated land is added. Open water is a significant fraction (>2 %) of the total area in only two subregions (Table 1): the Paraguay River subregion ($f_w = 0.089$), where the five largest lakes marked in Fig. 1 comprise much of the total open water, and the Nhecolândia subregion ($f_w = 0.062$), which has thousands of small lakes and ponds. In all subregions a significant area of flooded land (in addition to the open-water areas) usually persisted through the dry season, although the amount varied substantially among years. For example, in the Nabileque subregion at least 1000 km^2 of inundated floodplain persisted through the dry seasons from 1979–85, but low flooding in 1986 was followed by more severe desiccation by the end of that year, when only a few hundred km^2 remained inundated.

Differences in the timing of the inundation peaks among subregions are readily visible by comparing the monthly means from the SMMR time series (Fig. 6). The monthly minima and maxima are plotted together with the means

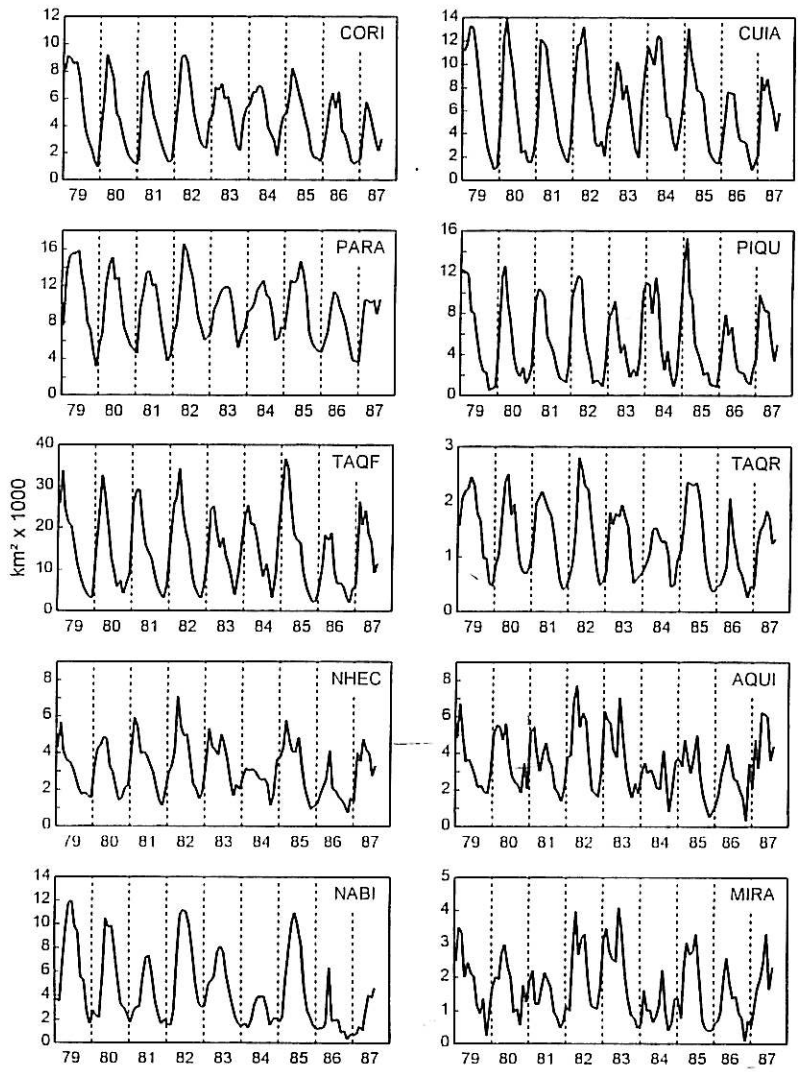

Fig. 5. Monthly estimates of inundation area for each subregion of the Pantanal, derived from the 1979–87 SMMR observations. Subregion abbreviations are defined in Fig. 1.

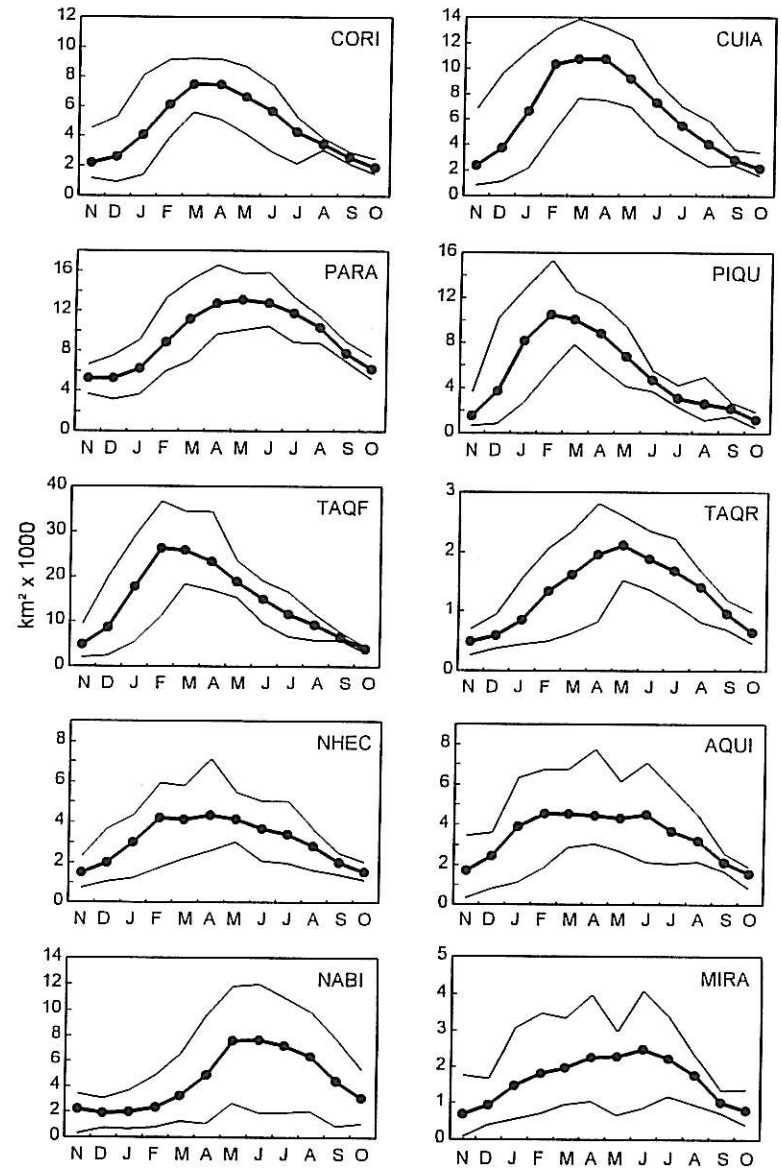

Fig. 6. Annual cycle of inundation area for each subregion of the Pantanal, derived from the 9-year time series in Fig. 5. Mean, maximum and minimum areas for each month are depicted. Subregion abbreviations are defined in Fig. 1.

to provide an indication of the interannual variability. Peak rainfall tends to occur from November–March in most of the region, as in the example in Fig. 3 (BRAZIL 1979). The monthly means in Fig. 6 show that inundation tends to peak from 2–6 months after the peak rainfall. There is a general progression of the flood wave along regional hydrologic flow paths, with the earliest flooding in northern and eastern parts of the Pantanal, followed by delayed flooding in the Paraguay River and Nabileque subregions, which receive water draining from the aforementioned areas. Nabileque provides the most dramatic example of delayed flooding, with maximum inundation corresponding with the beginning of the local dry season, 4–6 months after the peak rainfall.

The range between the minimum and maximum inundation in a particular month shows that in most subregions inundation area is particularly variable during the initial flooding and at maximum inundation, and is much less variable as the flood waters recede (Fig. 6). This reflects the variable timing and magnitude of the rainfall that produces the flooding. The ranges show that seasonal flooding patterns are particularly variable in the subregions of the southern Pantanal. Inundation of floodplains in the southern Pantanal that are contiguous with the floodplain of the Paraguay River, such as those of the Taquari River and Miranda subregions, may be variable in timing in part because inundation is controlled not only by overspill of the tributary rivers at high discharges, but also by impeded drainage due to the later impoundment by the delayed flood wave of the Paraguay River (SILVA & KUX 1992). In addition, the greater variability of flooding in the southernmost subregions (Miranda, Aquidauana/Negro, and Nabileque) reflects the less marked seasonality of rainfall in the uplands to the southeast (Serra da Bodoquena), where winter rains are more common (BRAZIL 1979).

Regional inundation patterns

Summation of the monthly observations of inundation area in each of the ten subregions yields a time series of inundation area for the entire Pantanal (Fig. 7). The upper limit of the ordinate reflects the total area (137,000 km^2). The area inundated at a particular time oscillated between approximately 11,000 and 110,000 km^2. There is no apparent relationship between the minimum and maximum inundation areas in a given seasonal cycle; the maximum inundation area in a particular year cannot be predicted from the previous minimum area, nor can the minimum area be predicted from the previous maximum area. The seasonal pattern of regional inundation is depicted by the monthly means (Fig. 8), which peak in March and April.

The total wetland area in the Pantanal is considerably greater than the peaks in Fig. 7 because of differences in the timing of inundation across the region. The total area subject to inundation in at least one month over the course

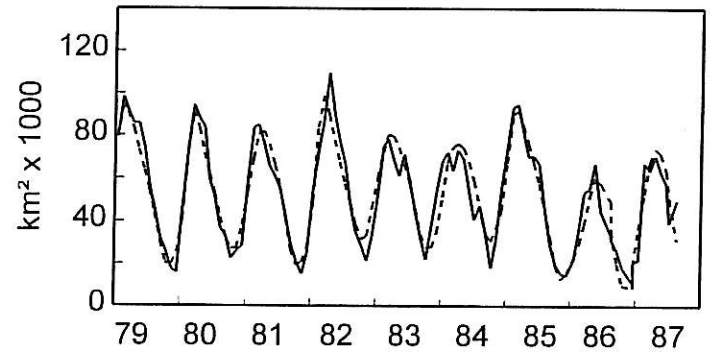

Fig. 7. Monthly estimates of total inundation area in the Pantanal (solid line), calculated by summation of the monthly estimates of inundation area in the subregions (Fig. 5). Monthly predictions of inundation area from the Paraguay River stage using equation (4) are shown by the dashed line.

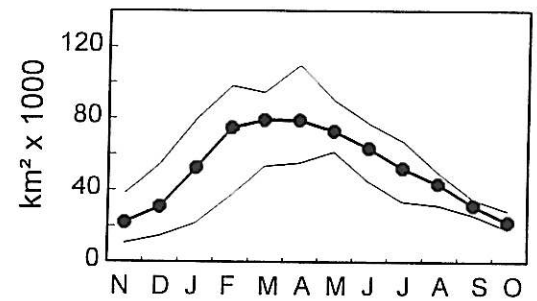

Fig. 8. Annual cycle of total inundation area in the Pantanal, derived from the time series in Fig. 6. Mean, maximum and minimum values for each month are depicted.

of the year is graphed in Fig. 9, which provides a measure of the extent of seasonal wetlands in the region. These data show that 90–95 % of the 137,000-km^2 area delineated in Fig. 1 was subject to inundation in 4 of the 9 years. In the dryest year of the series (1986), two-thirds of the total area was still subject to inundation at some month during the annual cycle.

Extension of the inundation record

The 9-year series of SMMR data analyzed in this study provides an indication of the recent interannual variability in inundation dynamics in the Pantanal, but more dramatic fluctuations in rainfall and inundation are known to occur in the region. A longer record of inundation dynamics can be reconstructed by relating inundation area to river stage. The longest record of river stage in the

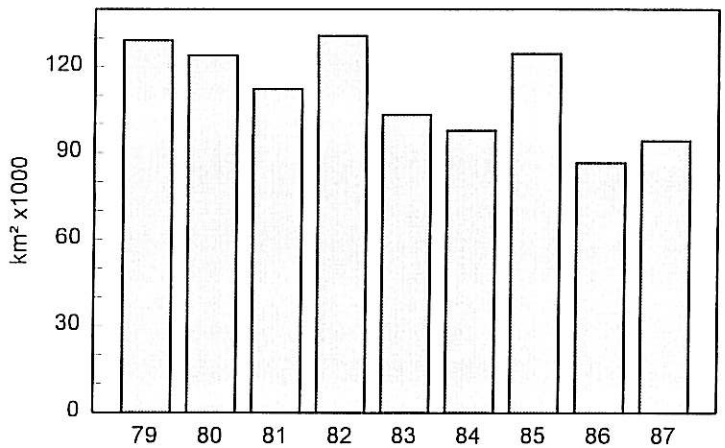

Fig. 9. Total area of the Pantanal that was subject to inundation in at least one month during the calendar year.

region is available for the Paraguay River at Ladário (near Corumbá), which began in 1900 (UNESCO 1973). The Paraguay River stage is appropriate for prediction of inundation area because of its central location in the Pantanal, and because the Paraguay River discharge reflects drainage from floodplains throughout the region.

A plot of the total inundation area (data in Fig. 7) against mean monthly stage at Ladário (data in Fig. 3) for the 9 years of SMMR observations reveals a strong clockwise hysteresis and is not well approximated by a single linear or curvilinear model (Pearson product-moment correlation coefficient $r=0.66$). Examination of a cross-correlation function plot for the two time series revealed that changes in river level tend to lag behind changes in inundation area by 1–2 months, which makes sense because the stage was measured at a point downriver from much of the inundable area. Correlation improved by introducing a lag of either 1 or 2 months in the stage data, but the best correlation was obtained between inundation area and the mean Paraguay River stage 1 and 2 months later (Pearson $r=0.95$). Linear regression produced the following equation ($P \leq 0.001$, $N=102$):

$$\hat{Y}_t = 18{,}520\,\bar{X}_{(t+1,t+2)} - 17{,}309 \qquad (4)$$

to predict inundation area in month t ($\hat{Y}_t$, in km^2) from the mean stage of the following two months ($\bar{X}_{(t+1,t+2)}$, in m). The standard error of the estimate is 7943 km^2. This model reproduces the salient features of seasonal and interannual fluctuations in inundation area, as depicted in Fig. 7, which compares the model predictions to the SMMR inundation area observations.

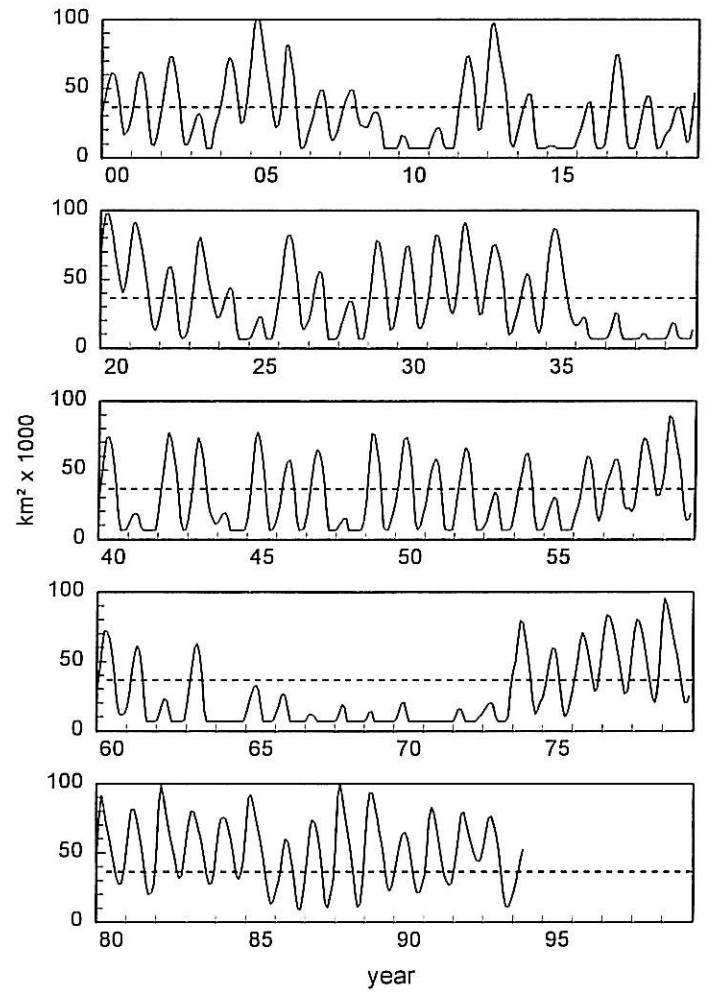

Fig. 10. Reconstruction of a 95-year time series of inundation area in the Pantanal, based on the observed correlation between inundation area and the stage of the Paraguay River at Ladário, near Corumbá. The inundation area was estimated at monthly intervals from mean monthly stage using equation (4) (stage data are from UNESCO (1973) and the Brazilian Navy at Ladário). The dashed line marks the overall mean of inundation area for 1900–94 (34,190 km^2).

Equation (4) was employed to reconstruct the fluctuations in inundation area in the Pantanal since 1900 (Fig. 10). The range in stage during this time period was similar to that observed during the 1979–87 period from which the

model was derived, except for occasional very low stages during dry periods. We lack SMMR observations of inundation area at stages <1.3 m, so for these dates we used a fixed value of 6770 km^2, which is the area predicted by (4) for a stage of 1.3 m.

The reconstructed record of inundation area in Fig. 10 reveals that in the past, interannual variability in inundation has been much larger than observed in the 9 years of SMMR observations. The overall mean of inundation area for 1900–94 is 34,190 km^2, and is depicted by the horizontal dashed line in Fig. 10. Relatively regular cycles of inundation and desiccation occurred throughout the period from 1974–93. Prior to 1974 there was a 10-year period of relatively dry conditions with little inundation. From 1900–64, interannual variability was large but multi-year cycles of wetter or drier conditions are less evident. As in the 9-year SMMR time series, prediction of the extent of inundation in a given year from the inundation of the previous year appears difficult.

Applications of the inundation observations

The inundation observations derived from the SMMR data are valuable for understanding the floodplain ecosystem because inundation is one of the key physical factors that control the biogeochemical cycles and ecological dynamics of the floodplain environment (Richey et al. 1991, Junk 1993). For example, emission from natural wetlands is a major source of atmospheric methane, a greenhouse gas that plays important roles in the regulation of climate (Cicerone & Oremland 1988). Significant emission occurs only during inundation, when anaerobic environments produce methane. Estimates of methane emission from tropical wetlands are important to our understanding of the global methane cycle, but they currently suffer from a lack of information on the extent and timing of inundation (Bartlett & Harriss 1993). The SMMR inundation observations could be combined with knowledge of the seasonal variation in emission rates from inundated land to improve estimates of the total emission of methane from floodplain environments.

The inundation observations provide insight into the seasonal and interannual fluctuations in habitat for economically important fishes as well as for wildlife that is affected by inundation. Variability in fish yields among years might be related to differences in inundation during the life history of the fishes (Welcomme 1985). Several endangered or threatened species of mammals and birds remain relatively abundant in the Pantanal (Mittermeier et al. 1990), including the jaguar (*Pantera onca*), which seeks dry refuges during inundation, and the giant otter (*Pteroneura brasiliensis*), which depends on inundated areas for food and protection. Improved information on inundation might help in the conservation of these species because their populations are likely to be regulated by occasional extreme floods or droughts.

Information on inundation is equally important for management of floodplains, and for minimizing the impact of flooding on human activities. Data on annual variation of natural flooding could prove valuable in present attempts to evaluate the environmental impact of a proposed river navigation project known as the Hidrovia, which would entail modifications of the Paraguay River channel throughout the Pantanal, with poorly understood implications for floodplain inundation (Ponce 1995). Improved prediction of inundation some months in advance would help to reduce the socioeconomic impacts of the natural variability. For example, the very dry period of 1964–73 corresponded with expansion of cattle ranching within the Pantanal, and the unforeseen return of high floods in 1974 resulted in large losses of cattle that could not be moved to higher ground before the floods arrived (Wilcox 1992). Prediction might be improved through consideration of the spatial and temporal variation in inundation area, which might be a better indicator of the progress of the flood wave than river level, which is monitored only along the major rivers.

Acknowledgments

This research was supported by the U.S. National Aeronautics and Space Administration (grant NAG W-2724) and the California Space Institute. We are grateful to Bhaskar Choudhury of NASA for the SMMR data set. Our field experience in the Pantanal was facilitated by the Centro de Pesquisa Agropecuária do Pantanal (CPAP-EMBRAPA) in Corumbá, Brazil. Our understanding of the hydrology of the region was enhanced by conversations with many EMBRAPA scientists, including Celso João Alves Ferreira, João Vila da Silva, Osni Corrêa de Souza, Débora Calheiros, Araê Boock and Sergio Galdino. The Brazilian Navy at Ladário provided recent river stage data.

References

Adámoli, J. (1982): O Pantanal e suas relações fitogeográficas com os cerrados: Discussão sobre o conceito de "Complexo do Pantanal". – Separata dos Anais do XXXII Congresso Nacional de Botânica (Universidade Federal de Piauí, Teresina, Brazil): 109–119.

Bartlett, K. B. & Harriss, R. C. (1993): Review and assessment of methane emissions from wetlands. – Chemosphere **26:** 261–320.

Brazil (1979): Relatório da Primeira Fase, Descrição Física e Recursos Naturais. Estudo de Desenvolvimento Integrado da Bacia do Alto Paraguai (Convênio Governo Brasileiro-UNDP-OEA) – Superintendência do Desenvolvimento da Região Centro-Oeste, Brasília.

– (1982): Projeto RADAMBRASIL, Levantamento de Recursos Naturais, Volume 27, Folha SE.21 Corumbá e Parte da Folha SE.20. – Ministerio das Minas e Energia, Brasília.

BUCHER, E. H., BONETTO, A., BOYLE, T., CANEVARI, P., CASTRO, G., HUSZAR, P. & STONE, T. (1993): Hidrovia: An initial environmental examination of the Paraguay-Paraná Waterway – Wetlands for the Americas, Manomet, Massachusetts: Publication Number 10.

CHOUDHURY, B. J. (1989): Monitoring global land surface using Nimbus-7 37 GHz data, theory and examples. – Int. J. Remote Sensing **10:** 1579–1605.

– (1991): Passive microwave remote sensing contribution to hydrological variables. – Surv. Geophys. **12:** 63–84.

– (1993): Reflectivities of selected land surface types at 19 and 37 GHz from SSM/I observations. – Remote Sensing Environ. **46:** 1–17.

CHOUDHURY, B. J., MAJOR, E. R., SMITH, E. A. & BECKER, F. (1992): Atmospheric effects on SMMR and SSM/I 37 GHz polarization difference over the Sahel. – Int. J. Remote Sensing **13:** 3443–3463.

CICERONE, R. J. & OREMLAND, R. S. (1988): Biogeochemical aspects of atmospheric methane. – Global Biogeochem. Cycles **2:** 299–327.

FU, C. C., HAN, D., KIM, S. T. & GLOERSEN, P. (1988): User's guide for the Nimbus 7 Scanning Multichannel Microwave Radiometer (SMMR) CELL-ALL tape – U.S. National Aeronautics and Space Administration, Washington, D.C.: Reference Publication 1210.

GIDDINGS, L. & CHOUDHURY, B. J. (1989): Observation of hydrological features with Nimbus-7 37 GHz data, applied to South America. – Int. J. Remote Sensing **10:** 1673–1686.

GLOERSEN, P., CAMPBELL, W. J., CAVALIERI, D. J., COMISO, J. C., PARKINSON, C. L. & ZWALLY, H. J. (1992): Arctic and Antarctic Sea Ice, 1978–1987: Satellite Passive-Microwave Observations and Analysis. – National Aeronautics and Space Administration, Washington, D.C.: NASA SP-511.

GLOERSEN, P., CAVALIERI, D. J., CHANG, A. T. C. et al. (1984): A summary of results from the first NIMBUS 7 SMMR observations. – J. Geophys. Res. **89** (D 4): 5335–5344.

HAMILTON, S. K., CORRÊA DE SOUZA, O. & COUTINHO, M. E. (In press): Dynamics of floodplain inundation in the alluvial fan of the Taquari River (Pantanal, Brazil). – Verh. Int. Verein. Limnol.

HAMILTON, S. K., SIPPEL, S. J. & MELACK, J. M. (1995): Oxygen depletion and carbon dioxide and methane production in water of the Pantanal wetland of Brazil. – Biogeochemistry **30:** 115–141.

HEYMSFIELD, G. M. & FULTON, R. (1992): Modulation of SSM/I microwave soil radiances by rainfall. – Remote Sensing Environ. **39:** 187–202.

HOLLINGER, J. P., PIERCE, J. L. & POE, G. A. (1990): SSM/I instrument evaluation. – IEEE Transact. Geosci. Remote Sensing **28:** 781–790.

JUNK, W. J. (1993): Wetlands of tropical South America. – In: WHIGHAM, D., DYKYJOVÁ, D. & HEJNÝ, S. (eds.): Wetlands of the World: Inventory, Ecology and Management, Volume I. – Kluwer (Dordrecht), pp. 679–739.

JUSTICE, C. O., TOWNSEND, J. R. G. & CHOUDHURY, B. J. (1989): Comparison of AVHRR and SMMR data for monitoring vegetation phenology on a continental scale. – Int. J. Remote Sensing **10:** 1607–1632.

KERR, Y. H. & NJOKU, E. G. (1993): On the use of passive microwaves at 37 GHz in remote sensing of vegetation. – Int. J. Remote Sensing **14:** 1931–1943.

KLAMMER, G. (1982): Die Paläowüste des Pantanal von Mato Grosso und die pleistozäne Klimageschichte der brasilianischen Randtropen. – Z. Geomorph. N. F. **26:** 393–416.

LILLESAND, T. M. & KIEFER, R. W. (1994): Remote Sensing and Image Interpretation. – John Wiley, New York.

MELACK, J. M., HESS, L. L. & SIPPEL, S. J. (1994): Remote sensing of lakes and floodplains in the Amazon Basin. – Remote Sensing Rev. **10:** 127–142.

MITTERMEIER, R. A., CÂMARA, I. G., PÁDUA, M. T. J. & BLANCK, J. (1990): Conservation in the Pantanal of Brazil. – Oryx **24:** 103–112.

PONCE, V. M. (1995): Hydrologic and environmental impact of the Paraná-Paraguay waterway on the Pantanal of Mato Grosso, Brazil, a reference study. – San Diego State University, San Diego, CA.

POTT, V. J., BUENO, N. C., PEREIRA, R. A. C., SALIS, S. M. & VIEIRA, N. L. (1989): Distribuição de macrófitas aquáticas numa lagoa na Fazenda Nhumirim, Nhecolândia, Pantanal, MS. – Acta Botanica Brasiliensia **3:** 153–168.

PRADO, D. E., GIBBS, P. E., POTT, A. & POTT, V. J. (1992): The Chaco-Pantanal transition in southern Mato Grosso, Brazil. – In: FURLEY, P. A., PROCTOR, J. & RATTER, J. A. (eds.): Nature and dynamics of forest-savanna boundaries. – Chapman and Hall, London, pp. 451–470.

PRANCE, G. T. & SCHALLER, G. B. (1982): Preliminary study of some vegetation types of the Pantanal, Mato Grosso, Brazil. – Brittonia **34:** 228–251.

RATTER, J. A., POTT, A., POTT, V. J., CUNHA, C. N. DA & HARIDASAN, M. (1988): Observations on woody vegetation types in the Pantanal and at Corumbá, Brazil. – Not. Royal Bot. Gard. Edinburgh **45:** 503–525.

RICHEY, J. E., VICTORIA, R. L., SALATI, E. & FORSBERG, B. R. (1991): The biogeochemistry of a major river system: The Amazon case study. – In: DEGENS, E. T., KEMPE, S. & RICHEY, J. E. (eds.): Biogeochemistry of Major World Rivers. – John Wiley, New York, pp. 57–74.

SILVA, J. S. V. & KUX, H. J. H. (1992): Thematic mapper and GIS data integration to evaluate the flooding dynamics within the Pantanal, Mato Grosso do Sul State, Brazil. – Proceedings of the 1992 International Geoscience and Remote Sensing Symposium. IEEE (Piscataway, New Jersey), pp. 1478–1480.

SIPPEL, S. J., HAMILTON, S. K. & MELACK, J. M. (1994): Determination of inundation area in the Amazon River floodplain using the SMMR 37 GHz polarization difference. – Remote Sensing Environ. **48:** 70–76.

SPENCER, R. W., GOODMAN, H. M. & HOOD, R. E. (1989): Precipitation retrieval over land and ocean with the SSM/I: Identification and characteristics of the scattering signal. – J. Atmospheric and Oceanic Techn. **6:** 254–273.

SUTCLIFFE, J. V. & PARKS, Y. P. (1987): Hydrological modelling of the Sudd and Jonglei Canal. – Hydrol. Sci. J. **32:** 143–159.

UNESCO (1973): Hydrological studies of the Upper Paraguay River basin (Pantanal). 1966–1972. – Technical Report/UNESCO/UNDP BRA66521, Paris.

WELCOMME, R. L. (1985): River fisheries. – Food and Agriculture Organization of the United Nations (Rome): FAO Fisheries Technical Paper 262.

WILCOX, R. (1992): Cattle and environment in the Pantanal of Mato Grosso, Brazil, 1870–1970. – Agricult. Hist. **66:** 232–256.

Submitted: 17 October 1995; accepted: 6 February 1996.